Wasit Journal of Engineering Sciences

Journal homepage: https://ejuow.uowasit.edu.iq

Non-invasive evaluation of blood flow through a healthy and stenosed coronary artery

Zahraa Ahmed Hamza[*1], Mohammed Ghalib Al-Azawy[1], Alaa Ahmed Alkinani[2]

Affiliations
[1]Department of Mechanical Engineering, Wasit University, Wasit, Iraq

[2]Al-Zahraa teaching Hospital, Wasit, Iraq

Correspondence
Zahraa Ahmed Hamza, Department of Mechanical Engineering, Wasit University, Wasit, Iraq
Email: Zahraaa301@uowasit.edu.iq

Received
26-August-2022
Revised
22-October-2022
Accepted
24-October-2022
Doi: 10.31185/ejuow.Vol10.Iss3.369

Abstract

The current numerical analysis was utilised to compare the hemodynamic effects caused by flow disruptions in coronary arteries with and without stenosis. Computational Fluid Dynamics (CFD) technique was used in order to evaluate the hemodynamic importance of patient-specific coronary stenosis and to provide information to the public, particularly surgeons, and assist them in reducing the risk of stenosis. Assuming the flow is turbulent and non-Newtonian viscosity, the Carreau model is incorporated by utilizing STAR-CCM+ 2021.2.1. The tested model is a patient-specific coronary stenosis with an area stenosis of (60%). The velocity, shear stress, and strain rate were evaluated and revealed that the stenosed artery experiences more hemodynamic impacts as the flow rate increases compared to the normal artery. To assess the turbulence effect, the turbulent kinetic energy (TKE) and the turbulent viscosity ratio (TVR) were applied. The findings showed that the TKE and TVR are almost the same downstream of the stenosis. The TKE and TVR being somewhat higher with the stenosed artery model than the unstenosed artery model, and it increases as the flow increases. Moreover, to determine the stenosis severity, the coefficient of pressure drop (CDP) and lesion flow coefficient (LFC) were used and showed that the CDP value be higher in stenosed artery (107pa) compared to a normal artery (5.2pa) but it was less when the flow increased (84.4pa), (2.5pa) respectively. Whereas the LFC value in the stenoses artery is higher (0.61) and rises as flow increases (0.69).

Keywords: Coronary stenosis, hemodynamic impacts, stenosis severity, computational fluid dynamics, non-Newtonian fluid flow, turbulent flow.

الخلاصة: ان التحليل العددي الحالي هو مقارنة التأثيرات الدورة الدموية الناتجه عن اضطرابات التدفق في الشرايين التاجيه مع التضييق و بدون التضييق من اجل تقييم اهمية الدوره الدموية لتضييق شريان تاجي لمريض بتقنية ديناميكيات السوائل العددية (CFD) لتقديم إرشادات للمجتمع، وخاصة الأطباء الجراحين، ومساعدتهم للحد من مخاطر الشريان المتضيق باستخدام برنامج (STAR-CCM+ 2021.2.1). بافتراض أن التدفق مضطرب ولزوجة غير نيوتونية باستخدام نموذج Carreau. يشتمل نموذج الاختبار على شريان تاجي متضيق لمريض خاص، ونسبة تضيق المساحة ٦٠%. تم التحقق وتقييم نتائج السرعة، إجهاد القص، ومعدل الإجهاد ، وكشف أن الشريان المتضيق يتعرض لتأثيرات ديناميكية أكبر مع زيادة معدل التدفق مقارنةً بـ الشريان الطبيعي TKE وTVR وايضا لوحظ ايضا ان نسبة اللزوجة المضطربة والطاقة الحركية المضطربة متماثلان تقريبًا في اتجاه مجرى التضيق ويكونان اعلى مع الشريان المتضيق مقارنة مع الشريان الغير متضيق ويزدادان بزيادة معدل التدفق ولتحديد شدة التضييق تم استخدام معامل انخفاض الضغط ومعامل تدفق حيث اضهرت النتائج ان انخفاض الضغط يكون اعلى في الشريان المتضيق (١٠٧باسكال) بينما في الشريان الطبيعي (٥,٢باسكال) وتكون هذه القيم اقل عند زيادة معدل التدفق (٨٤,٤باسكال) (٢,٥باسكال) على التوالي . اما بالنسبة لقيم معامل تدفق تكون اعلى في لبشريان المتضيق (٠,٦١) وتزداد بزيادة معدل التدفق لتصل الى (٠,٦٩).

1. INTRODUCTION

The biggest cause of death worldwide is cardiovascular disease (CVD), which is predicted to account for more than 22 million fatalities annually by 2030 [1]. Atherosclerosis, a disorder that causes inflammation in the arterial wall and narrows the lumen, is the primary degenerative mechanism that underlies CVDs [1]. Furthermore, a monthly report issued by Al-Zahraa teaching hospital in Wasit Governorate, Iraq, announced that about 740 clinical cardiac examinations and approximately 150 coronary angiography and angioplasty were performed every

month. In other words, atherosclerosis is a quiet, complex, and complicated disease that develops when immune cells and lipids build up in the artery wall, causing a plaque to form[2]. Local physiological, biomechanical, and systemic factors have all been linked to atherosclerosis , and local important parameters affect it. In particular, Wall Shear Stress (WSS) is a well-known indicator of the development of coronary atherosclerosis [3] [4]. High levels of WSS are associated with plaque destabilization even though low wall shear stress areas have been known to be more prone to plaque production [5].previously, the flow dynamics in presence of atherosclerosis do not significantly change, but as time passes, the transition to turbulence can occur even at much smaller Reynolds numbers; these deposits are critical in modifying the flow characteristics [6]. Numerous hemodynamic studies have been conducted to comprehend the flow field variations. Various measurement approaches can be used to do this in an in-vivo setting. Some hemodynamic variables, including wall shear stress, are still difficult to quantify with enough accuracy; because it enables the highly accurate calculation of a variety of hemodynamic parameters. Computational Fluid Dynamic (CFD) has already utilized as an essential substitute to thoroughly analyse a number of blood physical phenomena in blood vessels and as a crucial part of the study of CVDs [7],[2].

In addition to study the hemodynamics of blood flow, it is crucial to take into account the disease's worldwide effects. Due to this, substantial research in this field has been conducted using experimental and/or numerical techniques. Despite the fact that many experimental hemodynamic investigations have been conducted in the literature using in vivo or in vitro methods [8], there are several limitations that have been noted elsewhere [9]. as a result computational techniques have recently become the method of choice for many researchers [10][11], such as Young [12] examined the flow in a tube that was somewhat constricted using a rudimentary model in among the earliest thorough examinations of the flow in stenosis.

Due to the complexity of blood flowhemodynamics research has evolved significantly over time, and scientists have accepted a number of hypotheses. While some researchers looked at the turbulent transition [13] [7] and non-Newtonian impacts [14][15] and [6] . Laminar and Newtonian effects in coronary arteries were investigated [17] [18] [1]. Various investigations have underlined the significance of considering that blood is non-Newtonian behaviour and choosing the appropriate model to more accurately reflect the in vitro condition [18].

6 non-Newtonion models and a Newtonian model are evaluated in an intriguing study conducting by Razavi et al. [18]. The acquired data demonstrated that, when compared to other models, the power law model yields bigger variations, amplifying the non-Newtonion behaviour in terms of WSS and velocity values. However, the authors underestimate the non-Newtonian behaviour. In contrast, the modified Casson models and generalised power law are closer to the Newtonian state. The Carreau and Carreau-Yasuda models were demonstrated as the best models to replicate the behaviour of blood because they indicated moderate values as opposed to the preceding models (the cut-off value over which flow can be expressed to be non-Newtonian). Other authors have also compared Newtonian and non-Newtonian models [14] [15].

Although identical results were achieved for both scenarios in terms of velocity profiles and WSS measurements, Chaichana et al. [19] contrasted the influence of the power law generalized model (non-Newtonian) with the Newtonian fluid. On the other hand, the Newtonian and non-Newtonian Carreau-Yasuda models were contrasted by Gaudio et al.[20]. According to their findings, the velocity for such a Carreau-Yasuda model is marginally smaller than that in the Newtonian model; however, the non-Newtonian impacts are more significant in the distributions of shear stress indices. The Carreau and Carreau-Yasuda models are the most popular in research [11][21] , and Razavi et al.[18] also suggested that they are the best models to simulate blood rheology.

The flow of blood in arteries is typically laminar when there is no stenosis. But a zone of turbulent flow may develop downstream of a mild to severe stenosis. Jahngiri et al. [13] improved diagnostic techniques for locating a severe stenosis may result from greater comprehension of the flow and flow turbulence in the post-stenoses zone [22]. Mahalingam et al. [7] employed the SST $k-\omega$ model throughout pulsatile across coronary arteries with various degrees of stenosis to investigate the turbulent transition effect on haemodynamic variables. The results showed that after 50% stenosis, the transition to turbulent begins to occur, and above and beyond 70% stenosis, it becomes totally turbulent. The $k-\omega$ transitional has been examined and verified by numerous authors [23][7][1], and this model has been revealed as the best turbulence model to describe the flow of blood in pulsatile situations, according to the literature.

The Newtonian, pulsatile, and turbulence flow patterns in double stenoses were numerically examined by Lee et al. [24][25] with Reynolds numbers ranging from 100 to 4000. It was thought that constriction ratios and stenoses'

separation varied. After the turbulent flow was solved using a $k-\omega$ turbulence model, the flow field and secondary flow zones were examined. The first article [24] expected the artery to be stiff, while the second piece assumed it to be flexible. The Large Eddy Simulation (LES) method is suggested by Molla et al. [26] for investigations into the flow of blood in a narrowing artery. The authors presupposed that the flow was Newtonian pulsatile turbulent blood flow. More recently, Al-Azawy et al. [27] and Carvalho et al. [1] investigated the effects of non-Newtonian models and turbulence models as part of the ongoing effort. These articles claim that for a large portion of the flow through medical devices like blood pumps and arteries, the turbulence model with elliptic blending Reynolds stress model with the Carreua model provided the most perfect prediction.

Furthermore, it must be noted that now in clinical practice, it is impossible to perform a physical examination for patients just on their WSS values[28] As a result, the diagnostic criteria utilized by doctors have a larger practical purpose than has been adequately addressed in the literature to date. The most often utilized diagnostic variables are fractional flow reserves (FFR), coefficient of pressure drop (CDP), and lesion flow coefficient (LFC) [29][30][31][32]. In a 3D straight artery model, Kamangar et al. [33] examined the effects of various stenosis shapes and porous vessel wall materials using coronary diagnostic criteria. The findings came to the conclusion that varied stenosis morphologies and porous medium could result in incorrect evaluation of the stenosis's diagnosis, particularly with regard to FFR. Additionally, it is difficult to precisely regulate how to measure FFR in practice when it depends on where the guide wire is placed [34]. Whereas with CDP and LFC, the examination will be more accurate, especially when it comes to the intermediate states of stenosis.

The aim of the present work is to compare the hemodynamic effects caused by flow disruptions in coronary arteries with and without stenosis in order to evaluate the hemodynamic importance of patient-specific coronary stenosis by using a Carreau model.

1.1 Problem statement

The narrowed arteries could block blood flow and form clots, or thrombosis. In medical applications, the range of area stenosis (40%-70%) is intermediate stenosis and requires further examination by the cardiologist to determine whether the patient requires an angioplasty or if medication is sufficient. In order to assess the level of these problems and reduce the risk, the blood was investigated numerically in the present work.

2.1. PHYSICAL MODEL

In this work, a model of special data of a patient from the AL-Zahraa teaching hospital at Wasit, Iraq with a stenosis in the left coronary artery was performed as illustrated in figure 1. The area of stenosis for this case is 60%. In the present work, this case is compared with a healthy left coronary artery (without narrowing) (see figure 2, which presents the geometry of both cases).

Figure 1. Coronary angiography with geometrical data.

(a) Three- diamention model

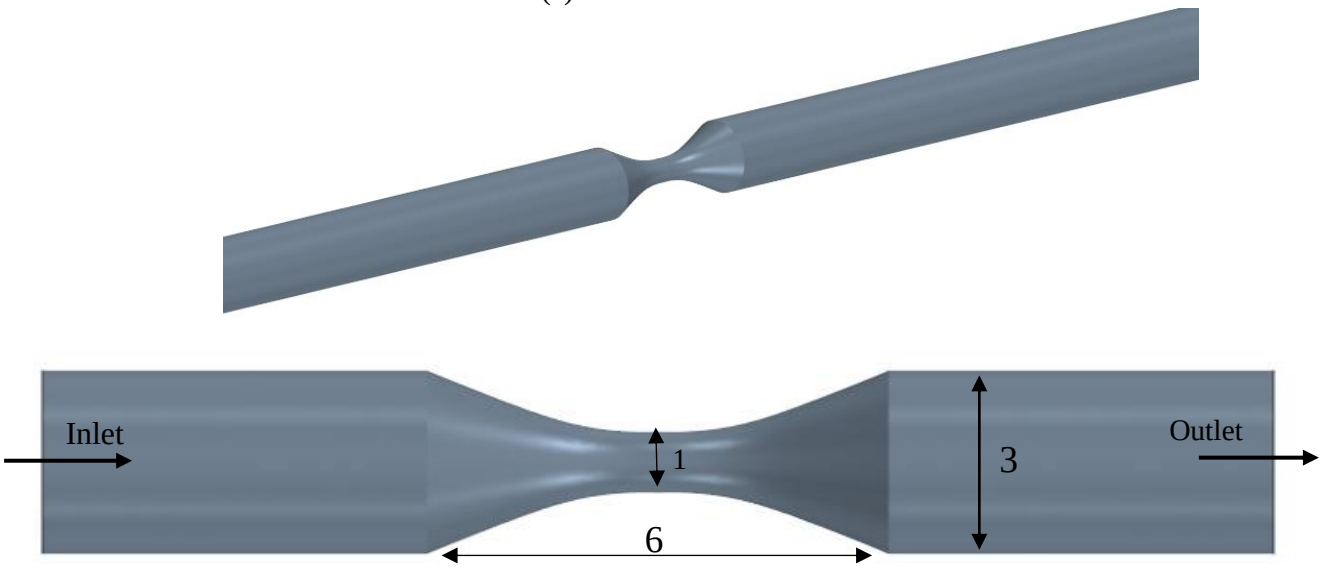

(b) Dimensions of the stenosis artery

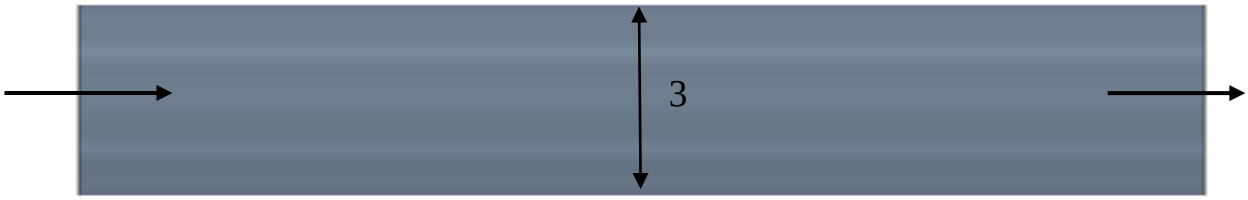

(c) Dimensions of the healthy artery

Figure 2. Geometry of models (all dimensions are in millimetres (mm)).

2.2. **NUMERICAL DESCRIPTION**

Using the commercial CFD software STAR-CCM+ 2021.2.1 (16.04.012-R8) [35], a numerical model of the 3D computational geometry of a stenosis artery was created. Furthermore, the polyhedral mesh that is suitable for complex geometry is included in this software. The steady Navier-Stokes equations are fixed numerically using a finite volume methods in this software [36], as shown below.

$$\frac{\partial u_i}{\partial x_i} = 0 \tag{1}$$

$$\rho u_j \frac{\partial u_i}{\partial x_j} = -\frac{\partial p}{\partial x_i} + \frac{\partial}{\partial x_j} \left[\mu(s) \frac{\partial u_i}{\partial x_j} - \overline{u_i u_j} \right] \tag{2}$$

Where u_i is the change in velocity, u_i = (u , v, w), is the Cartesian coordinate, x_i = (x, y, z); while p is the pressure and ρ is the density (1060 kg/m^3) , $\overline{u_i u_j}$ is the Reynolds stress tensor, $\mu(s)$ is the blood viscosity, which is calculated from the shear rate tensor [36] as follows:

$$|S| = \sqrt{2\,S_{ij}\,S_{ij}} \qquad \text{Where} \quad S_{ij} = \frac{1}{2}\left(\frac{\partial u_i}{\partial x_j} + \frac{\partial u_j}{\partial x_i}\right) \tag{3}$$

As indicated in Table 1, five variable meshes were created to examine the spatial mesh resolution demands for the 3D simulators. The CFD model in this study was created with a polyhedral mesh using STARCCM+ 2021.2.1 (16.04.012-R8) [35], as illustrated in Figure 3. In addition, four prism layers were used to deal with the boundary layer.

Table 1 Data of mesh.

Mesh	**M1**	**M2**	**M3**	**M4**	**M5**
Number of cell	125466	326726	859145	1092156	1377140

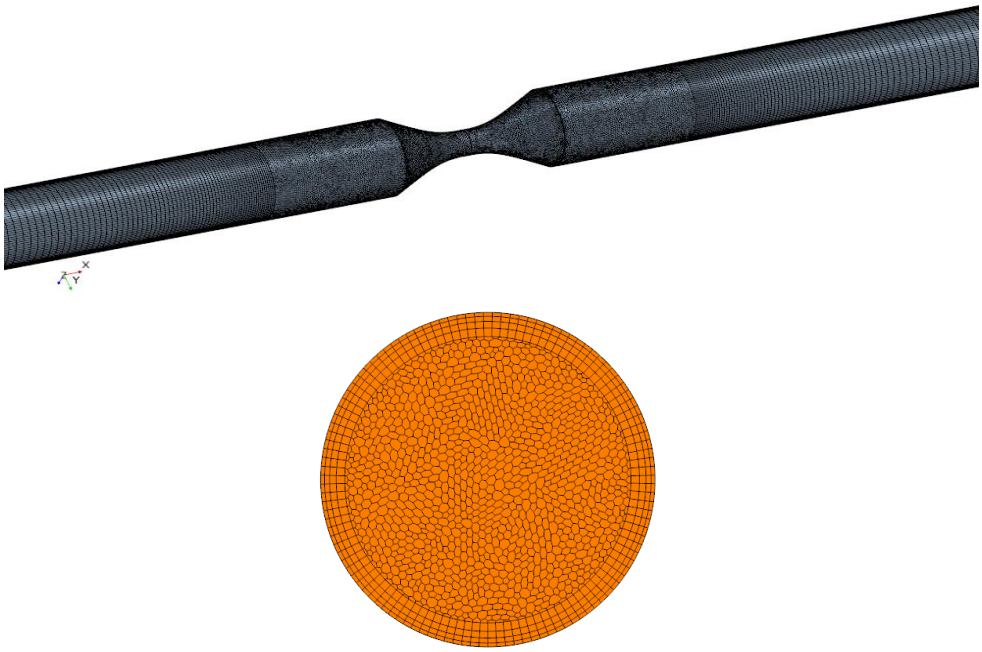

Figure 3. Mesh arrangements showing the prism layer.

Figure 4 shows the behavior of axial velocity at a horizontal line across a stenosis region, demonstrating a grid-independency test. The velocity forecasts for meshes M4 and M5 are roughly comparable to the other three meshes, as illustrated in this graph. As a result, the mesh M4 (1092156 cells) is selected to represent the fluid characteristics across the model for the following simulation.

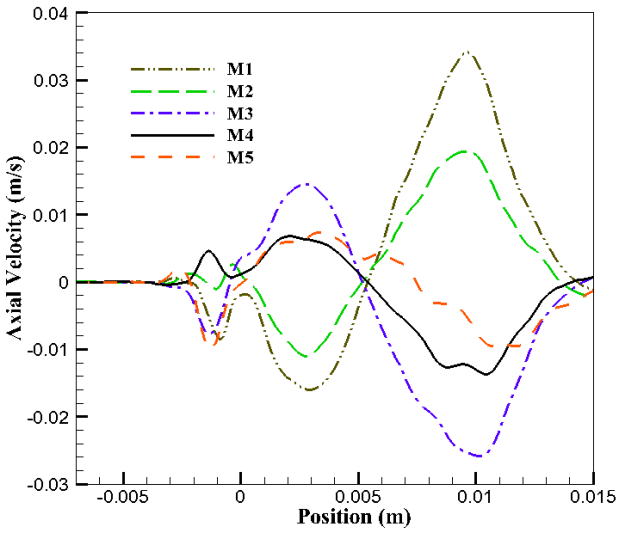

Figure 4. Sketch of Axial velocity through a horizontal centreline.

The near-wall sharpness was calculated using distance in non-dimensional space to the first grid cell next to a wall:

$$y^+ = \frac{y}{\mu}\sqrt{\rho\tau_w} \tag{4}$$

Here y is the distances between that cell's centre and the wall, μ the viscosity of blood, ρ the density of the blood, and τ_w is the wall shear stress [35], as shown in figure 5. Furthermore, the flow chart in figure 6 depicts the series of operations carried out by the CFD solver of the present work.

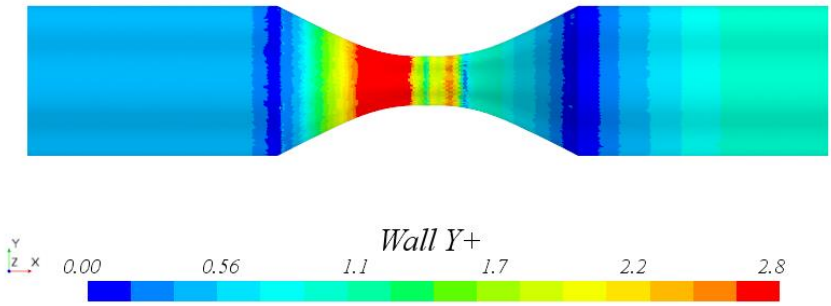

Figure 5. Contour of non-dimensional distance to the first near-wall grid point y^+.

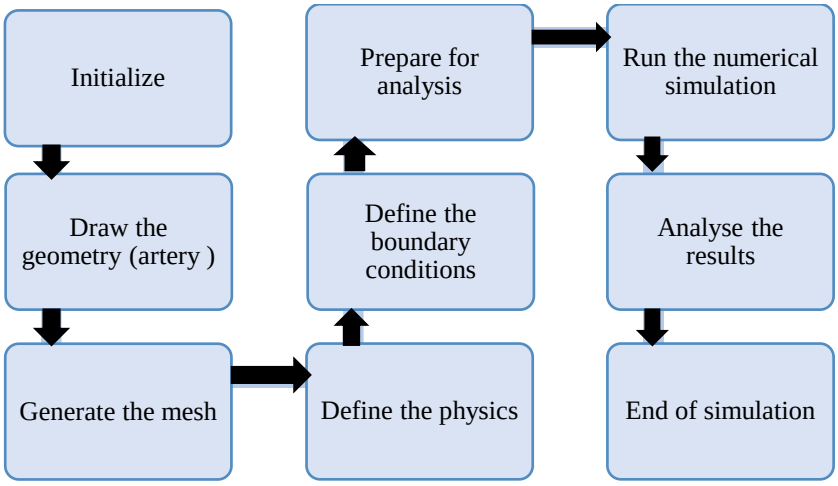

Figure 6. A flowchart depicting the CFD setup process**.**

2.3. **MODELLING OF BLOOD RHEOLOGY AND TURBULENCE**

It was supposed that blood did not behave like a Newtonian fluid flow. As previously investigated in [37][38], it is critical to use a suitable non-Newtonian model for blood flow analysis in order to get good findings.

The Carreau model produces more realistic findings when simulating blood flow, and it is widely used in hemodynamic studies [18] when compared to other non-Newtonian models.

The Carreau model is shaped like this equation [39]:

$$\mu(|S|) = \mu_\infty + (\mu_0 - \mu_\infty)[1 + (\lambda S)^2]^{(n-1)/2} \quad (4)$$

Table 2 contains the data of the variables that appear in the preceding equation.

Table 2. Parameters used with Carreau approach [39].

Blood viscosity at zero shear rate, μ_0	Blood viscosity at infinite shear rate, $\mu\infty$	The relaxation time, λ	The constant model, n
0.056 Pa s	0.00345 Pa s	3.313	0.3568

Turbulence modeling is significant in hemodynamics investigations because the flow can become turbulent in the presence of stenosis, resulting in the creation of recirculation zones [40]. Considering the influence of turbulence in arteries with narrowing plays a vital role in predicting the real difficulties that occur from this change in arterial area. As a result, the elliptic blending Reynolds stress model was adopted in this work[40][41], since it has superior capabilities, especially with low Reynolds numbers[42].

2.4. **BOUNDARY CONDUCTIONS**

A human heart continuously beats faster and slower in response to stressors and alterations in the environment, so in the present work, the velocity was applied at the inlet utilizing two values of velocity flow rate, Q = 85 ml/min (0.2 m/s) at rest and Q = 255 ml/min (0.6 m/s) at hyperemic [43]. A non-slip condition was applied at the artery wall, and a zero pressure was specified at the outlet. The details of the present simulation are presented in table 3 for two cases; the first one is AS = 0%, while the second case is AS = 60%.

Table 3. Conditions that applied at the inlet.

Condition	Condition 1: at rest	Condition 2: at exercise
Flow rate (units)	85(ml/min)	255(ml/min)
Velocity at the inlet (unit)	0.2(m/s)	0.6(m/s)

3. RESULTS AND DISCUSSION

3.1. EXAMINATION OF FLOW FIELD

By comparison with the experimental results of a nozzle published by the Food and Drug Administration (FDA) [44], the present numerical simulation's axial velocity was first verified viewed in figure 7 . The axial velocity data were provided at a line placed at the outflow part, as shown in this figure. This figure shows high compatibility with the experimental findings of **[44]**. Thus, the maximum percent error between the simulation result model of viscosity (Carreau) and the experimental data, which is found from the result of **[44],** is 2.5%.

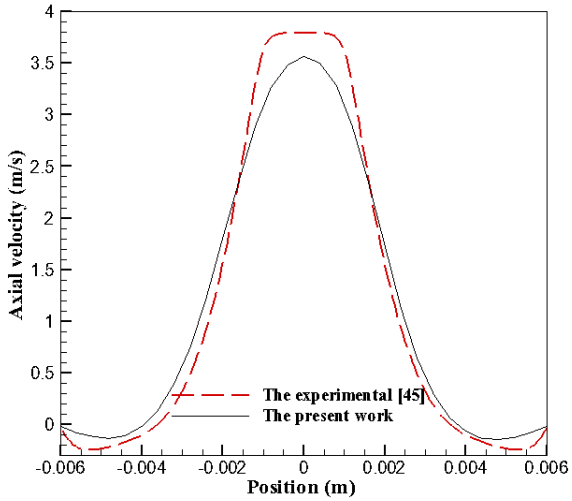

Figure 7. Axial velocity variation at the present work's line and experimental data from [44].

One of the most essential indicators for identifying the plaque-effected section of the coronary arteries is the velocity of blood flow, as shown in figure 8, which indicates the contour of velocity magnitude in (m/s) of a healthy artery (AS = 0%) and the stenosed artery (AS = 60%) at different flowrates.

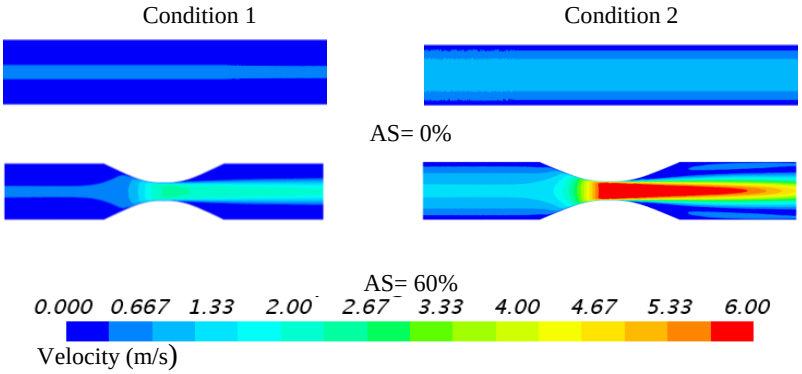

Figure 8. Contour of velocity magnitude at mid plane.

When compared to the normal left coronary artery from figure 8, the velocity across the stenoseis portion was found to be much higher. Also, an enhanced flow pattern was found in the stenosis artery as compared to the normal coronary artery over the plaque region when the flow rate was increased. However, a recirculation region was also identified immediately after the stenosis part. That results in increased plaque development; however, in the case of a normal coronary artery, a smooth velocity was found.

In the stenosis areas, there is a high blood flow velocity. Due to the smaller lumen diameter, the increased velocity causes greater blood flow resistance and reduced blood flow. This information could be extremely useful to medical professionals in locating hotspots wherein blood tends to collect. Furthermore, blood flow in the plaque-effected region is restricted, resulting in an imbalance in oxygen demand and supply in the tissue. Another of the main reasons for chest discomfort and other symptoms of coronary heart disease is the diminished oxygen delivery to the surrounding tissues.

3.2. CLINICAL ISSUES

For the cases that were analysed, the strain rate's clinical significance is presented with different flowrates, noticing that the values of strain rate are higher in the stenosis model than in the healthy model, and it is predicted to be higher when increasing the flowrate as presented in figures 10. It should be noted that the narrowing region is where the strain rate has its maximum value, which is likely to produce hemolysis.

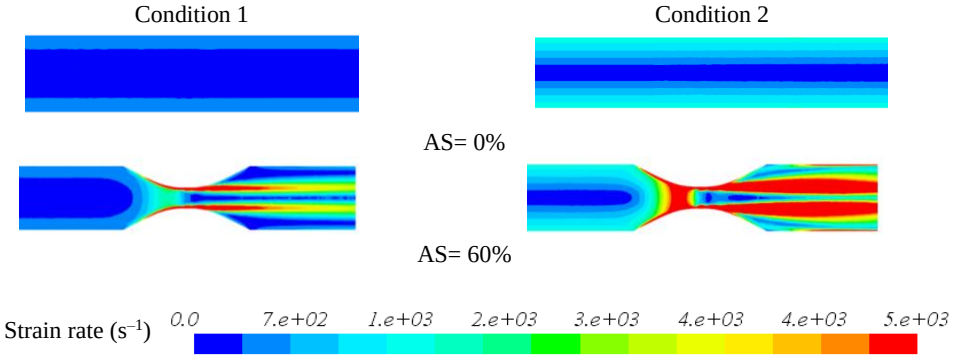

Figure 10. Contour of strain rate at mid plane.

Furthermore, the magnitude of Wall Shear Stress (WSS) is presented in figure 11. From this figure, it can be seen that regardless of the healthy model used, the WSS distribution on the wall follows a similar pattern. Where the flow accelerates substantially, where the vessel geometry shows acute curvature and creases, stresses are higher in value in stenosis arteries.

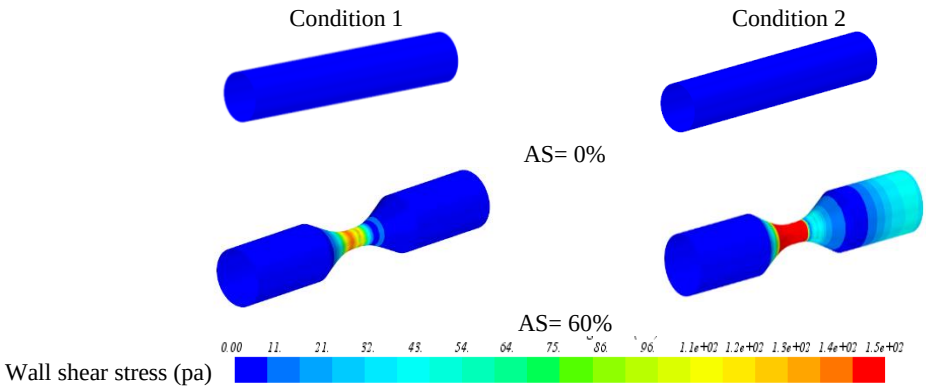

Figure 11. Contour of wall shear stress at the artery wall.

The degree of stenosis has a big influence on the WSS outcomes. The temporal variations in hemodynamic loads exerted on the artery wall are measured by the WSS gradient. The readings are significantly higher in stenosis areas than in unstenosis areas. In the healthy model, the WSS magnitude distribution data is shown to not exceed 10 pa, while WSS magnitude results in diseased models reach 150 pa. The WSS magnitude distribution findings vary in the stenosis area/s compared to unstenosis sections. WSS is highest at the neck (stenosis) and rises downstream following the stenosis as the flow becomes highly disrupted by the obstruction.

3.3. EFFECTS OF TURBULANCE

As stenosis progresses, the turbulent kinetic energy (TKE) value increases abruptly, as shown in Figure 12, indicating the transition to turbulence and the formation of turbulent structures downstream of the stenosis. The sudden increase in velocity leads to the development of turbulent structures. In addition, as shown in figure 13, the Turbulent Viscosity Ratio (TVR) is higher in the stenosis artery and it increases as the flow increases.

Furthermore, the turbulent kinetic energy is depicted before and after the stenosis in distinct vertical lines, as shown in figures 14 and 15. In a similar vein, the Turbulent Viscosity Ratio (TVR) was studied and shown in Figures 16 and 17. For both artery models, it can be noticed that the TKE and TVR are almost the same downstream of the stenosis, with the TKE being somewhat higher with the stenosis artery model than the unstenosis artery model, and it increases as the flow increases also. The TVR is higher in the stenosis artery model than the unstenosis artery model. The high velocity across and upstream of the stenosis causes this. The peak TKE comes downstream of the stenosis due to viscosity oscillations, especially when it is far away from the stenosis.

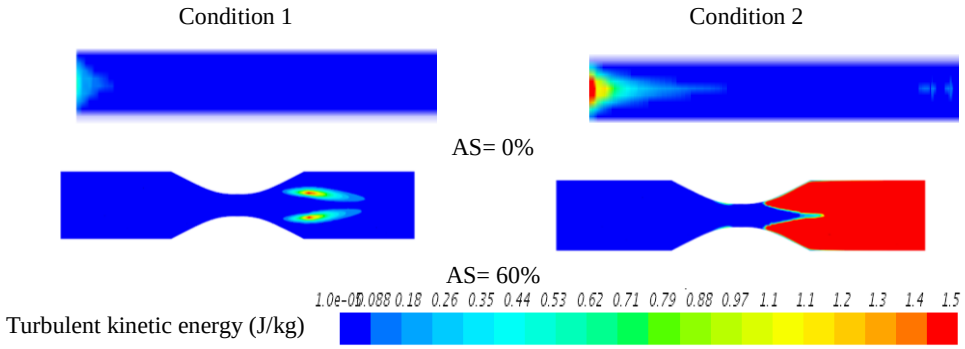

Figure 12. Contour of turbulent kinetic energy at mid plane.

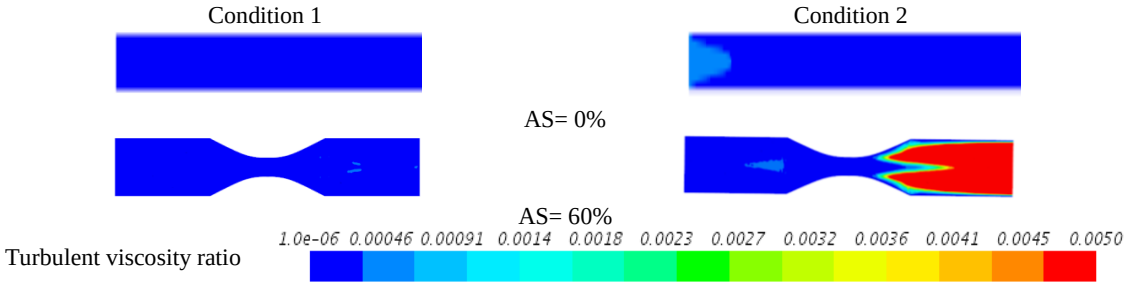

Figure 13. Contour of turbulent viscosity ratio at mid plane.

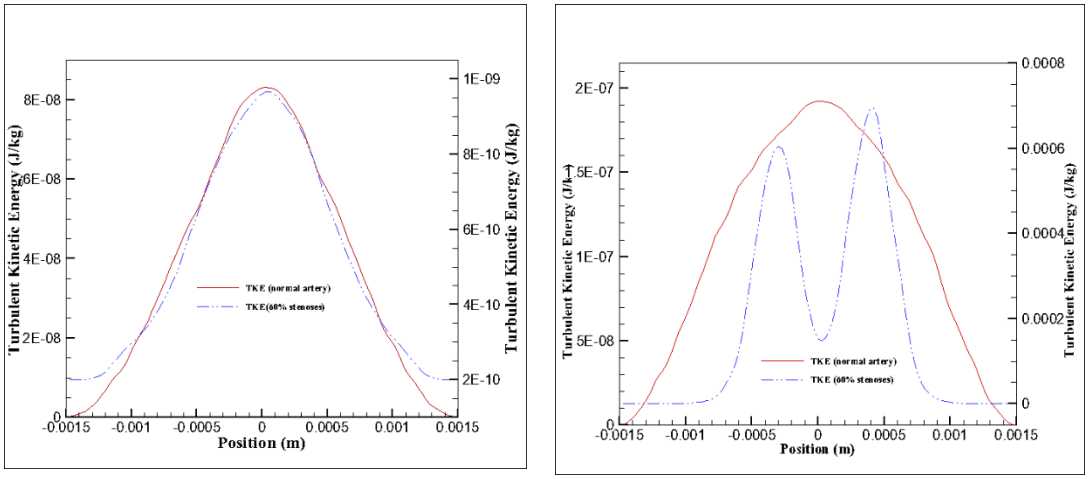

Before the stenosis (at x= -5mm) After the stenosis (at x= 5mm)

Figure 14. Plot of turbulent kinetic energy for two cases at different position at condition 1.

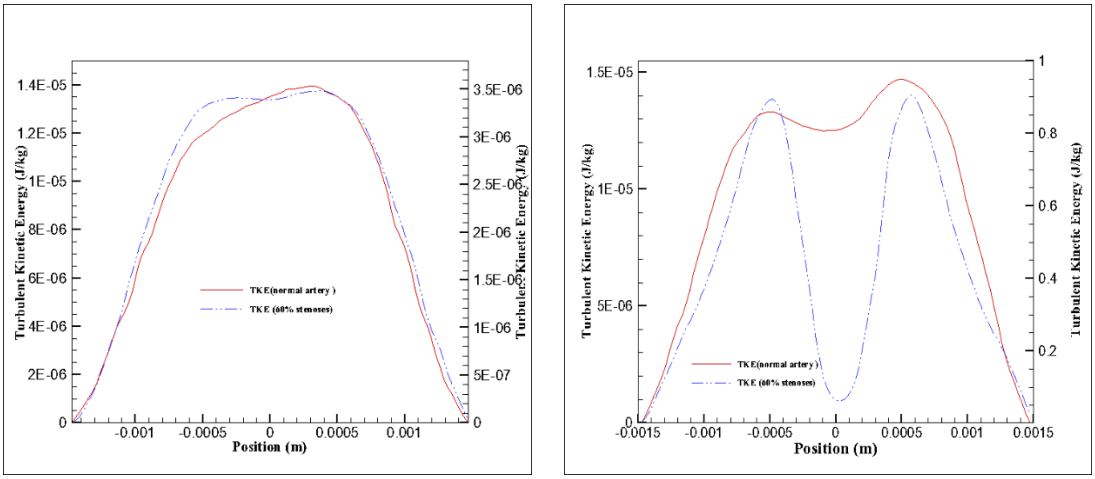

Before the stenosis (at x= -5mm) After the stenosis (at x= 5mm)

Figure 15. Plot of turbulent kinetic energy for two cases at different position at condition 2.

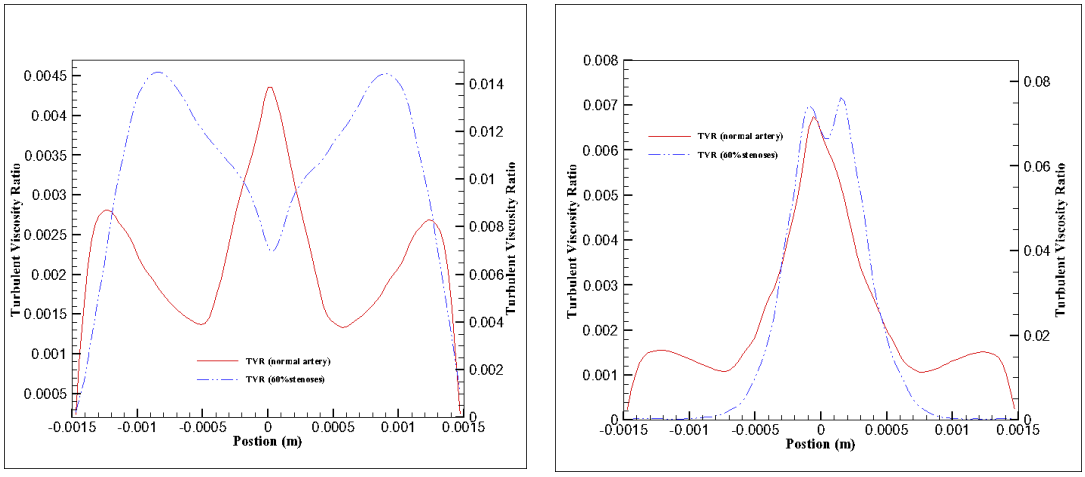

Before the stenosis (at x= -5mm) After the stenosis (at x= 5mm)

Figure 16. Plot of turbulent viscosity ratio for two cases at different position at condition 1.

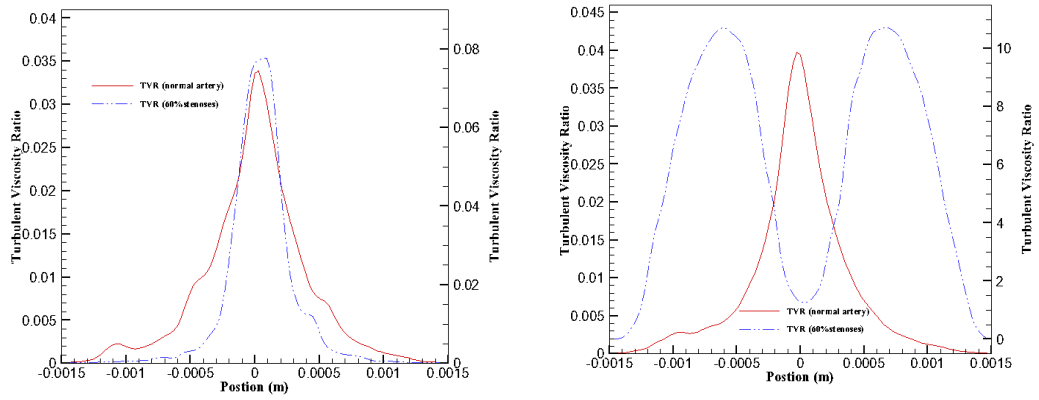

Before the stenosis (at x= -5mm) After the stenosis (at x= 5mm)

Figure 17. Plot of turbulent viscosity ratio for two cases at different position at condition 2.

3.4. EFFECT OF NON-NEWTONIAN

3.4.1. IMPORTANCE FACTOR

The clinical significance of the Importance Factor (IF) for the instances studied is analysed as suggested by [28]

$$IF = \frac{\mu(S)}{\mu_\infty} \qquad (5)$$

Where $\mu(S)$ is the real dynamic viscosity of blood, which is specified by the non-Newtonian models, where μ_∞ denotes the Newtonian shear viscosity ($\mu_\infty = 0.00345\ pa.s$).

The Newtonian flow will have an IF equal to 1, while non-Newtonian flow zones will be indicated by values that are different from unity. As shown in figure 18 the IF is bigger in the 0% blockage than in the 60% blockage, which means that the $\mu(S)$ is higher than the μ_∞ which means that the flow is non-Newtonian. In the 60% blockage, the flow is more Newtonian.

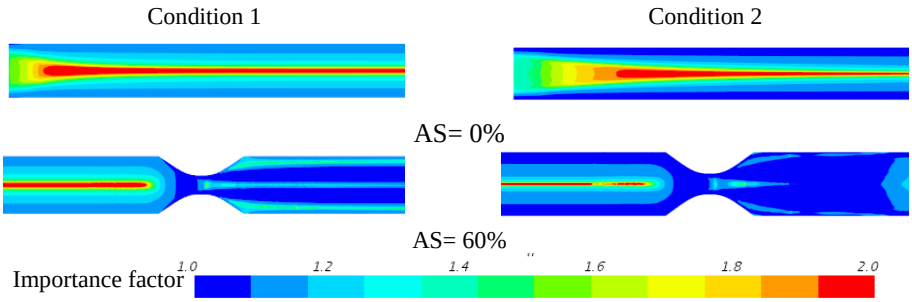

Figure 18. Contour of importance factor

As shown in Figure 19, the apparent blood viscosity variations with shear rate were investigated by comparing the findings of the Newtonian and Carreau models. When the shear rate is greater than 1000 1/s, the dynamic viscosity is virtually constant, as shown in this diagram.

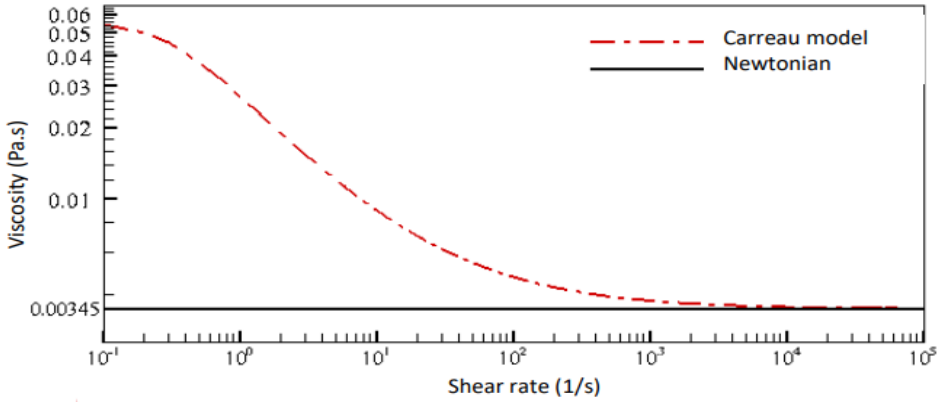

Figure.19 Viscosity of blood for Newtonian model and Carreau models versus strain rate.

5. Diagnostic Criteria

5.1. COFFECIENT OF PRESSURE DROP (CDP)

For determining the stenosis severity, the functional parameter CDP is based on the trans-stenosis pressure drop and velocity magnitude in the proximal part of the stenosis [30]. The CDP is defined as follows:

$$CDP = \frac{\Delta p}{0.5\ \rho v_e^2} \tag{6}$$

Where Δp is the pressure drops, $\Delta p = (p_{proximal} - p_{distal})$, v_e is the velocity proximal of the stenosis and ρ is the fluid density.

As the stenosis becomes more severe, the amount of distal pressure and flow (velocity) drops, and Δp rises. As the severity of the stenosis rises, the value of CDP expected to rise.

5.2. LESION FLOW COFFICENT (LFC)

The LFC is a standardized parameter whose value varies from 0 to 1, and it could be beneficial in clinical settings similar to the CDP. It integrates anatomical and functional endpoints, such as lesion geometry and pressure and flow data. The velocity value inside the throat area is used to define it. As the severity of the stenosis rises, the value of LFC is projected to rise [30].

$$LFC = \frac{1-K}{\sqrt{\Delta p / 0.5\rho\, v_m^2}} \quad (7)$$

Where $K = A_s/A_e$; A_s is the throat area of stenosis, v_s the velocity at throat region. The values of CDP and LFC for the present conditions were presented in table 4.The results show the CDP value decreases as the flow increases, but it rises as the degree of stenosis increases. While the LFC value increases as the flow increases and also increases as the stenosis severity increases.

Table 4. The results of CDP and LFC.

Area stenosis%	**At** Condition 1		**At** Condition 2	
	CDP (pa)	LFC	CDP(pa)	LFC
0%	5.2	0	2.5	0
60%	107	0.61	84.4	0.69

6. CONCLUSION

The goal of the current numerical analysis was to compare the hemodynamic effects caused by flow disruptions in coronary arteries with and without stenosis in order to evaluate the hemodynamic importance of patient-specific coronary stenosis. Assuming the flow is turbulent and non-Newtonian viscosity, a Carreau model was used. In this work, the mesh was constructed using commercial CFD software. Apart from the simplicity of the arterial stenosis model investigated here, the authors think that the simulation outcomes that the paper presents could provide a cardiologist or medical surgeon with a better understanding and in-depth knowledge of the significant fluid dynamics aspects of atherosclerosis that are typically present in a real-life biological stenosis.

An evaluation of the velocity, wall shear stress, and strain rate revealed that the stenosed artery experiences more hemodynamic impacts as the flow rate increases compared to the normal artery. Findings on the turbulent kinetic energy and turbulent viscosity ratio are almost the same downstream of the stenosis, with the TKE and TVR being somewhat higher with the stenosed artery model than with the unstenosis artery model, and that increases as the flow increases. Moreover, to determine the stenosis severity, the coefficient of pressure drop (CDP) and lesion flow coefficient (LFC) were used, showing that the CDP value is higher in a stenosed artery compared to a normal artery, but it is less when the flow increases. whereas in stenosed arteries, the LFC value is higher and rises as flow increases.

REFERENCES

1. Carvalho, V., Rodrigues, N., Lima, R. A., & Teixeira, S. (2020). Numerical simulation of blood pulsatile flow in stenotic coronary arteries: The effect of turbulence modeling and non-Newtonian assumptions. *Proceedings - 24th International Conference on Circuits, Systems, Communications and Computers, CSCC 2020*, 112–116. https://doi.org/10.1109/CSCC49995.2020.00027
2. Carvalho, V., Pinho, D., Lima, R. A., Teixeira, J. C., & Teixeira, S. (2021). Blood flow modeling in coronary arteries: A review. *Fluids*, *6*(2). https://doi.org/10.3390/fluids6020053
3. Toivari, M., Nygård, Y., Kumpula, E. P., Vehkomäki, M. L., Benčina, M., Valkonen, M., … Wiebe, M. G. (2012). Metabolic engineering of Saccharomyces cerevisiae for bioconversion of d-xylose to d-xylonate. *Metabolic Engineering*, *14*(4), 427–436. https://doi.org/10.1016/j.ymben.2012.03.002
4. Lopes, D., Puga, H., Teixeira, J., & Lima, R. (2020). Blood flow simulations in patient-specific geometries of the carotid artery: A systematic review. *Journal of Biomechanics*, *111*, 110019. https://doi.org/10.1016/j.jbiomech.2020.110019
5. De Nisco, G., Hoogendoorn, A., Chiastra, C., Gallo, D., Kok, A. M., Morbiducci, U., & Wentzel, J. J. (2020). The impact of helical flow on coronary atherosclerotic plaque

development. *Atherosclerosis*, *300*(December 2019), 39–46. https://doi.org/10.1016/j.atherosclerosis.2020.01.027
6. Moreno, C., & Bhaganagar, K. (2013). Modeling of stenotic coronary artery and implications of plaque morphology on blood flow. *Modelling and Simulation in Engineering*, *2013*. https://doi.org/10.1155/2013/390213
7. Mahalingam, A., Gawandalkar, U. U., Kini, G., Buradi, A., Araki, T., Ikeda, N., … Suri, J. S. (2016). Numerical analysis of the effect of turbulence transition on the hemodynamic parameters in human coronary arteries. *Cardiovascular Diagnosis and Therapy*, *6*(3), 208–220. https://doi.org/10.21037/cdt.2016.03.08
8. Kabinejadian, F., Ghista, D. N., Su, B., Kaabi Nezhadian, M., Chua, L. P., Yeo, J. H., & Leo, H. L. (2014). In vitro measurements of velocity and wall shear stress in a novel sequential anastomotic graft design model under pulsatile flow conditions. *Medical Engineering and Physics*, *36*(10), 1233–1245. https://doi.org/10.1016/j.medengphy.2014.06.024
9. Friedman, M. H., & Giddens, D. P. (2005). Blood flow in major blood vessels - Modeling and experiments. *Annals of Biomedical Engineering*, *33*(12 SPEC. ISS.), 1710–1713. https://doi.org/10.1007/s10439-005-8773-1
10. Fatahian, E., Kordani, N., & Fatahian, H. (2018). The application of computational fluid dynamics (CFD) method and several rheological models of blood flow: A review. *Gazi University Journal of Science*, *31*(4), 1213–1227.
11. Zakaria, M. S., Zainudin, S. H., Abdullah, H., Yuan, C. S., Latif, M. J. A., & Osman, K. (2019). CFD Simulation of Non-Newtonian Effect on Hemodynamics Characteristics of Blood Flow through Benchmark Nozzle. *Journal of Advanced Research in Fluid Mechanics and Thermal Sciences*, *64*(1), 117–125.
12. Young, D. F. (1968). Effect of a time-dependent stenosis on flow through a tube. *Journal of Manufacturing Science and Engineering, Transactions of the ASME*, *90*(2), 248–254. https://doi.org/10.1115/1.3604621
13. Jahangiri, M., Saghafian, M., & Sadeghi, M. R. (2015). Numerical simulation of hemodynamic parameters of turbulent and pulsatile blood flow in flexible artery with single and double stenoses. *Journal of Mechanical Science and Technology*, *29*(8), 3549–3560. https://doi.org/10.1007/s12206-015-0752-3
14. Doost, S. N., Zhong, L., Su, B., & Morsi, Y. S. (2016). The numerical analysis of non-Newtonian blood flow in human patient-specific left ventricle. *Computer Methods and Programs in Biomedicine*, *127*, 232–247. https://doi.org/10.1016/j.cmpb.2015.12.020
15. Apostolidis, A. J., Moyer, A. P., & Beris, A. N. (2016). Non-Newtonian effects in simulations of coronary arterial blood flow. *Journal of Non-Newtonian Fluid Mechanics*, *233*, 155–165. https://doi.org/10.1016/j.jnnfm.2016.03.008
16. Abbasian, M., Shams, M., Valizadeh, Z., Moshfegh, A., Javadzadegan, A., & Cheng, S. (2020). Effects of different non-Newtonian models on unsteady blood flow hemodynamics in patient-specific arterial models with in-vivo validation. *Computer Methods and Programs in Biomedicine*, *186*, 105185. https://doi.org/10.1016/j.cmpb.2019.105185
17. Amir Hossain Golshirazi, Etemad, S. G., & Javanbakht, V. (2020). Three-Dimensional Numerical Investigation of Steady State and Physiologically Realistic Pulsatile Flow through the Left Coronary Curved Artery with Stenosis. *Theoretical Foundations of Chemical Engineering*, *54*(3), 489–499. https://doi.org/10.1134/S0040579520030045
18. Razavi, A., Shirani, E., & Sadeghi, M. R. (2011). Numerical simulation of blood pulsatile flow in a stenosed carotid artery using different rheological models. *Journal of Biomechanics*, *44*(11), 2021–2030. https://doi.org/10.1016/j.jbiomech.2011.04.023
19. Chaichana, T., Sun, Z., & Jewkes, J. (2012). Computational fluid dynamics analysis of

the effect of plaques in the left coronary artery. *Computational and Mathematical Methods in Medicine*, *2012*, 1–9. https://doi.org/10.1155/2012/504367

20. Gaudio, L. T., Caruso, M. V., De Rosa, S., Indolfi, C., & Fragomeni, G. (2018). Different Blood Flow Models in Coronary Artery Diseases: Effects on hemodynamic parameters. *Proceedings of the Annual International Conference of the IEEE Engineering in Medicine and Biology Society, EMBS*, *2018-July*, 3185–3188. https://doi.org/10.1109/EMBC.2018.8512917
21. Pandey, R., Kumar, M., & Srivastav, V. K. (2020). Numerical computation of blood hemodynamic through constricted human left coronary artery: Pulsatile simulations. *Computer Methods and Programs in Biomedicine*, *197*, 105661. https://doi.org/10.1016/j.cmpb.2020.105661
22. Mittal, R., Simmons, S. P., & Udaykumar, H. S. (2001). Application of large-eddy simulation to the study of pulsatile flow in a modeled arterial stenosis. *Journal of Biomechanical Engineering*, *123*(4), 325–332. https://doi.org/10.1115/1.1385840
23. Zhang, J., Zhang, P., Fraser, K. H., Griffith, B. P., & Wu, Z. J. (2013). Comparison and Experimental Validation of Fluid Dynamic Numerical Models for a Clinical Ventricular Assist Device. *Artificial Organs*, *37*(4), 380–389. https://doi.org/10.1111/j.1525-1594.2012.01576.x
24. Lee, T. S., Liao, W., & Low, H. T. (2003). Numerical simulation of turbulent flow through series stenoses. *International Journal for Numerical Methods in Fluids*, *42*(7), 717–740. https://doi.org/10.1002/fld.550
25. Lee, T. S., Liao, W., & Low, H. T. (2004). Numerical study of physiological turbulent flows through series arterial stenoses. *International Journal for Numerical Methods in Fluids*, *46*(3), 315–344. https://doi.org/10.1002/fld.755
26. Molla, M. M., Paul, M. C., & Roditi, G. (2010). LES of additive and non-additive pulsatile flows in a model arterial stenosis. *Computer Methods in Biomechanics and Biomedical Engineering*, *13*(1), 105–120. https://doi.org/10.1080/10255840903062545
27. Ziervogel, G., Cartwright, A., Tas, A., Adejuwon, J., Zermoglio, F., Shale, M., & Smith, B. (2008). Climate change and adaptation in African agriculture. *Training*, *4179*, 53. https://doi.org/10.1002/cnm
28. Mynard, J. P., Wasserman, B. A., & Steinman, D. A. (2013). Errors in the estimation of wall shear stress by maximum Doppler velocity. *Atherosclerosis*, *227*(2), 259–266. https://doi.org/10.1016/j.atherosclerosis.2013.01.026
29. Kolli, K. K., Helmy, T. A., Peelukhana, S. V., Arif, I., Leesar, M. A., Back, L. H., … Effat, M. A. (2014). Functional diagnosis of coronary stenoses using pressure drop coefficient: A pilot study in humans. *Catheterization and Cardiovascular Interventions*, *83*(3), 377–385. https://doi.org/10.1002/ccd.25085
30. Peelukhana, S. V., Back, L. H., & Banerjee, R. K. (2009). Influence of coronary collateral flow on coronary diagnostic parameters: An in vitro study. *Journal of Biomechanics*, *42*(16), 2753–2759. https://doi.org/10.1016/j.jbiomech.2009.08.013
31. Konala, B. C., Das, A., & Banerjee, R. K. (2011). Influence of arterial wall-stenosis compliance on the coronary diagnostic parameters. *Journal of Biomechanics*, *44*(5), 842–847. https://doi.org/10.1016/j.jbiomech.2010.12.011
32. Peelukhana, S. V., Banerjee, R. K., van de Hoef, T. P., Kolli, K. K., Effat, M., Helmy, T., Arif, I. (2018). Evaluation of lesion flow coefficient for the detection of coronary artery disease in patient groups from two academic medical centers. *Cardiovascular Revascularization Medicine*, *19*(3), 348–354. https://doi.org/10.1016/j.carrev.2017.08.018
33. Kamangar, S., Kalimuthu, G., Anjum Badruddin, I., Badarudin, A., Salman Ahmed, N. J., & Khan, T. M. Y. (2014). Numerical investigation of the effect of stenosis geometry

on the coronary diagnostic parameters. *Scientific World Journal*, *2014*. https://doi.org/10.1155/2014/354946
34. Abhijit Sinha Roy, Lloyd H. Back, R. K. B. (2006). Guidewire flow obstruction effect on pressure drop-flow relationship in moderate coronary artery stenosis.
35. STAR-CCM+. (2020). STAR-CCM+ Documentation Theory Guide, Turbulence. *Siemens,GER*.
36. Levy, S. W. (1959). *Use of Madribon in Dermatological Conditions, With Special Reference To Acne*. *Annals of the New York Academy of Sciences* (Vol. 82). https://doi.org/10.1111/j.1749-6632.1959.tb44882.x
37. Al-Azawy, M. G., Kadhim, S. K., & Hameed, A. S. (2020). Newtonian and non-newtonian blood rheology inside a model of stenosis. *CFD Letters*, *12*(11), 27–36. https://doi.org/10.37934/cfdl.12.11.2736
38. Johnston, B. M., Johnston, P. R., Corney, S., & Kilpatrick, D. (2004). Non-Newtonian blood flow in human right coronary arteries: steady state simulations. *Journal of biomechanics*, *37*(5), 709–720. https://doi.org/10.1016/j.jbiomech.2003.09.016
39. Kadhim, S. K., Al-Azawy, M. G., Ali, S. A., & Kadhim, M. Q. (2021). The influence of non-Newtonian model on properties of blood flow through a left coronary artery with presence of different double stenosis. *International Journal of Heat and Technology*, *39*(3), 895–905. https://doi.org/10.18280/ijht.390324
40. Manceau, R., & Hanjalić, K. (2002). Elliptic blending model: A new near-wall Reynolds-stress turbulence closure. *Physics of Fluids*, *14*(2), 744–754. https://doi.org/10.1063/1.1432693
41. Lardeau, S., Manceau, R., Lardeau, S., & Manceau, R. (2016). Computations of canonical and complex flow configurations using a robust formulation of the elliptic-blending Reynolds-Stress model.
42. Al-Azawy, M. G., Turan, A., & Revell, A. (2016). Assessment of turbulence models for pulsatile flow inside a heart pump. *Computer methods in biomechanics and biomedical engineering*, *19*(3), 271–285. https://doi.org/10.1080/10255842.2015.1015527
43. Li, S., Chin, C., Thondapu, V., Poon, E. K. W., Monty, J. P., Li, Y., … Barlis, P. (2017). Numerical and experimental investigations of the flow–pressure relation in multiple sequential stenoses coronary artery. *International Journal of Cardiovascular Imaging*, *33*(7), 1083–1088. https://doi.org/10.1007/s10554-017-1093-3
44. Hariharan, P., Giarra, M., Reddy, V., Day, S. W., Manning, K. B., Deutsch, S., … Malinauskas, R. A. (2011). Multilaboratory particle image velocimetry analysis of the FDA benchmark nozzle model to support validation of computational fluid dynamics simulations. *Journal of Biomechanical Engineering*, *133*(4), 1–14. https://doi.org/10.1115/1.4003440